Journal of Engineering Mathematics **30**: 97–118, 1996.

Integral formulation to simulate the viscous sintering of a two-dimensional lattice of periodic unit cells

G.A.L. VAN DE VORST*
Department of Mathematics and Computing Science, Eindhoven University of Technology, P.O. Box 513, 5600 MB Eindhoven, The Netherlands

Received 23 March 1995

Abstract. In this paper a mathematical formulation is presented which is used to calculate the flow field of a two-dimensional Stokes fluid that is represented by a lattice of unit cells with pores inside. The formulation is described in terms of an integral equation based on Lorentz's formulation, whereby the fundamental solution is used that represents the flow due to a periodic lattice of point forces. The derived integral equation is applied to model the viscous sintering phenomenon, *viz.* the process that occurs (for example) during the densification of a porous glass heated to such a high temperature that it becomes a viscous fluid. The numerical simulation is carried out by solving the governing Stokes flow equations for a fixed domain through a Boundary Element Method (BEM). The resulting velocity field then determines an approximate geometry at a next time point which is obtained by an implicit integration method. From this formulation quite a few theoretical insights can be obtained of the viscous sintering process with respect to both pore size and pore distribution of the porous glass. In particular, this model is able to examine the consequences of microstructure on the evolution of pore-size distribution, as will be demonstrated for several example problems.

1. Introduction

A method to produce glass fibres for the telecommunications industry is heating a porous pure glass to a sufficiently high temperature so that the glass becomes a highly viscous fluid: the flow causes densification of the glass. The driving force for this phenomenon is the excess of free surface energy of the porous glass compared to a same quantity of a fully dense glass. This process is usually referred to as *viscous sintering*. The glass flow appears to be highly viscous, incompressible and Newtonian: the Stokes creeping flow equations hold (cf. Kuiken [1] and Van de Vorst [2]). In general, the starting porous pure glass is produced by the so-called *sol-gel technique* (cf. Brinker and Scherer [3]); therefore the porous glass will also be referred to as the *gel*.

Ideally, this way one wants to produce a dense and homogeneous glass, free from voids and impurities. Therefore, a good theoretical understanding is needed of the densification kinetics of the porous glass, i.e. the viscous sintering phenomenon. In particular, one is interested in the shrinkage rate of the glass as a function of the viscosity and particle size, which reflects how time, temperature and microstructure influence the development of the densification process. Another question is what kind of structural configuration leads to a higher densification rate.

A simple approach to describing the sintering phenomenon is to consider the behaviour of simple systems only, i.e. so-called *unit problems* like the coalescence of two cylinders or two spheres. Such unit problems can be used to understand the behaviour of macroscopic systems. This approach goes back to 1945, when Frenkel [4] described the early stage of the coalescence of two equal spherical particles. He introduced the empirical rule, which is

* Present Address: Department of Systems Research and Development, DLO Agrotechnological Research Institute (ATO-DLO), P.O. Box 17, 6700 AA Wageningen, The Netherlands.

used in most mathematical models of viscous sintering to date, that the work done by surface tension in decreasing the total surface area is equal to the total energy produced by dissipation of the flow.

In the last few years a lot of work has been done in simulating the sintering of two-dimensional and axisymmetric unit problems. By now the evolution of some particular geometries can be solved even analytically, in particular using conformal mapping techniques, cf. Hopper [5]-[7].

The first numerical simulation of a unit problem of viscous sintering was carried out by Ross *et al.* [8]. They considered the sintering of an infinite line of equal cylinders and performed their simulation by employing a Finite Element Method (FEM). Jagota and Dawson [9]-[11] applied the FEM to simulate two axisymmetric problems, i.e. the coalescence of two equal spheres and of an infinite line of equal spheres. In Jagota and Dawson [10], the calculated behaviour of the two coalescing spheres is used to simulate the densification of a powder compact. In that paper, the particle packing is modelled as a framework of links between any pair of touching spheres and the growth of those links is described by considering the behaviour of each pair of coalescing spheres separately.

Kuiken [1] considered two-dimensional domains with a rather moderately varying curvature. He used an integral formulation based on the stream function and vorticity function and solved the resulting equations by employing a Boundary Element Method (BEM). In earlier work, cf. Van de Vorst *et al.* [12]-[15], we reported about the solution of the problem for arbitrarily shaped two-dimensional fluid regions with holes inside. In those papers, the Stokes problem is described by an integral formulation based on boundary distributions of single- and double-layer hydrodynamic potentials, which goes back to Lorentz [16].

A more sophisticated approach to describe the sintering phenomenon is the determination of a *representative unit cell* within the gel and to consider its densification. This unit cell has to be chosen so that it reflects the sintering of the porous glass as a whole realistically. Such a unit cell may consist of a number of particles, depending on the structure of the compact; this cell is also referred to as a *meso-cell* (De With [17]). Examples of this approach are the densification models developed by Mackenzie and Shuttleworth [18] and Scherer [19].

The model of Mackenzie and Shuttleworth [18] (MS-model) is generally accepted for late-stage viscous sintering. In this model, the densification results from the shrinkage of uniform spherical pores distributed throughout the gel. Hence the MS-model is also referred to as the *closed-pores model.* The representative unit cell is an individual spherical pore for which the flow field can be calculated analytically. The MS-model leads to an equation for the sintering time necessary to reach a particular density of the gel.

Scherer [19] developed the so-called *open-pores model*, that assumes the gel to be a regular three-dimensional array of interconnected liquid cylinders, and considered its shrinkage. This model was used by Scherer to analyze the early and intermediate stage of the sintering of gels. For the unit cell that represents this structure, Scherer took a cubic array consisting of intersecting cylinders on all the edges, from which the total surface was calculated. After applying Frenkel's energy balance, he obtained an analytical relationship between the relative density and the time. However, the model breaks down when a pore is trapped in each cell, in the late sintering stage. Scherer's main result is a graph showing the density of the gel as a function of time which is very close to the predicted densification rate of the MS-model.

In this paper, we present a mathematical formulation that can be used to simulate the densification of a two-dimensional arbitrarily shaped unit cell *numerically.* Therefore, it is assumed that the structure of the gel can be described by a periodic continuation of this

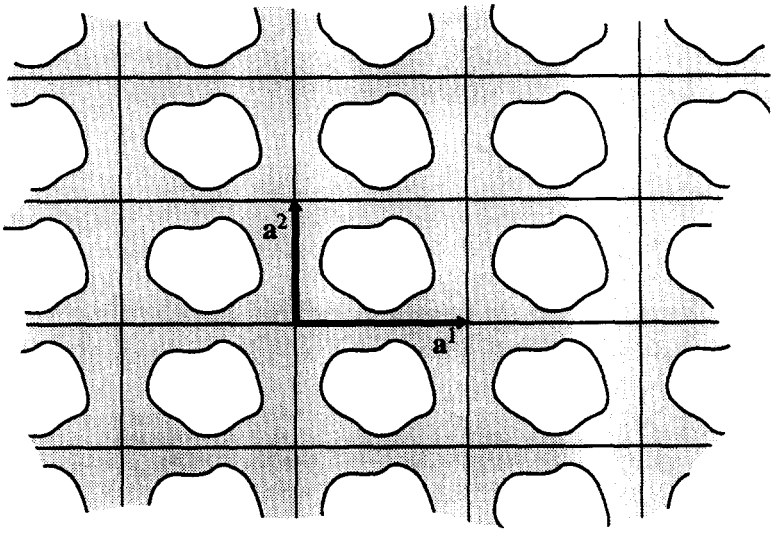

Fig. 1. The basic vectors of the unit cell of a periodic two-dimensional Stokes fluid lattice.

particular unit cell as time evolves. The flow of the pores in the unit cell will be described in terms of an integral equation based on Lorentz's formulation. However, as fundamental solution in this equation the solution of the Stokes problem for a two-dimensional lattice of point forces is used, derived by Hasimoto [20] for the three-dimensional case. Note that the three-dimensional formulation is already applied to investigate the behaviour of suspensions, cf. Brady *et al.* [21] and Pozrikidis [22]. In section 2, we outline the derivation of this fundamental solution in terms of a rapidly converging series. The derivation of the governing integral formulation is briefly discussed in section 3. The numerical solution of this formulation is based on the two-dimensional numerical code developed by us earlier, cf. Van de Vorst *et al.* [12]-[15]. Hence, the BEM is applied to solve the governing integral equations for a fixed domain. After solving the flow problem, time stepping is carried out by an implicit time integrator: a variable-step, variable-order Backward-Differences-Formulae (BDF) scheme. Finally, we will demonstrate the usefulness of this approach in obtaining more details about the viscous sintering phenomenon by considering some example problems.

2. Fundamental solution for a lattice of point forces

In this section we outline the derivation of the fundamental solution for a lattice of point forces in a two-dimensional plane in terms of a rapidly converging series, by roughly following the approach of Hasimoto [20].

Let $\mathbf{a}^1$ and $\mathbf{a}^2$ be the time dependent basic vectors of the unit cell of the lattice (see Fig. 1). Hence the position of the λ^{th} lattice is given by

$$\mathbf{X}^{\lambda} = \lambda_1 \mathbf{a}^1 + \lambda_2 \mathbf{a}^2 \qquad (\lambda_i = 0, \pm 1, \pm 2, \dots). \tag{2.1}$$

In analogy with the derivation of the fundamental solution for a point force in an infinite fluid (cf. Lorentz [16]), we seek the vector field $\mathbf{u}^m$ and the scalar function q^m that satisfies the following Stokes problem and continuity equation,

$$\begin{aligned} \Delta \mathbf{u}^m - \operatorname{grad} q^m &= \sum_{\lambda} \delta(\mathbf{x} - \mathbf{X}^{\lambda}) \mathbf{e}^m \\ \operatorname{div} \mathbf{u}^m &= 0. \end{aligned} \tag{2.2}$$

Here $m = 1$ or 2, $\mathbf{e}^m$ with $e_i^m = \delta_{im}$, is the m^{th} unit vector of an arbitrarily chosen Cartesian coordinate system, and $\delta(\mathbf{x})$ is the *Dirac delta function.* Moreover, the summation symbol used in Eq. (2.2) is an abbreviation for the double sum with respect to both λ_1 and λ_2 over all negative and positive integers. Physically, the above equations may be interpreted as the velocity at $\mathbf{x}$ induced by a two-dimensional lattice of unit point forces in the $\mathbf{e}^m$-direction concentrated at the points $\mathbf{X}^{\lambda}$.

Following Hasimoto [20], we may expand $\mathbf{u}^m$ and $(\operatorname{grad} q^m)$ by means of a Fourier series due to the periodicity of the flow field, thus

$$\mathbf{u}^m = \sum_{\mu} \hat{\mathbf{u}}_{\mu}^m \exp(-i\,\mathbf{x} \cdot \mathbf{K}^{\mu}) \quad \text{and} \quad -\operatorname{grad} q^m = \sum_{\mu} \hat{\mathbf{q}}_{\mu}^m \exp(-i\,\mathbf{x} \cdot \mathbf{K}^{\mu}), \tag{2.3}$$

where $\cdot$ denotes the inner product and $\mathbf{K}^{\mu}$ is a vector in the reciprocal lattice space and is equal to

$$\mathbf{K}^{\mu} = \mu_1 \mathbf{b}^1 + \mu_2 \mathbf{b}^2 \qquad (\mu_i = 0, \pm 1, \pm 2, \dots). \tag{2.4}$$

The vectors $\mathbf{b}^1$ and $\mathbf{b}^2$ are the basic vectors of the unit cell of the reciprocal lattice which are defined as

$$\mathbf{b}^1 = \frac{2\pi}{\tau}\left(a_2^2, -a_1^2\right)^{\mathrm{T}}, \qquad \mathbf{b}^2 = \frac{2\pi}{\tau}\left(-a_2^1, a_1^1\right)^{\mathrm{T}}, \tag{2.5}$$

and τ is the total surface area of one cell, i.e. $\tau = a_1^1 a_2^2 - a_1^2 a_2^1$. It can easily be seen that the following relation is satisfied between the basic vectors of the original and the reciprocal lattice,

$$\mathbf{a}^i \cdot \mathbf{b}^j = 2\pi \delta_{ij}. \tag{2.6}$$

After substitution of both the Fourier series (2.3) and the equality

$$\sum_{\lambda} \delta(\mathbf{x} - \mathbf{X}^{\lambda}) = \frac{1}{\tau} \sum_{\mu} \exp(-i\,\mathbf{K}^{\mu} \cdot \mathbf{x}), \tag{2.7}$$

in Eq. (2.2), we obtain the following relations for the coefficients $\hat{\mathbf{u}}_{\mu}^m$ and $\hat{\mathbf{q}}_{\mu}^m$,

$$-k^2 \hat{\mathbf{u}}_{\mu}^m + \hat{\mathbf{q}}_{\mu}^m = \frac{\mathbf{e}^m}{\tau}, \tag{2.8}$$

$$\mathbf{K}^{\mu} \cdot \hat{\mathbf{u}}_{\mu}^m = 0, \tag{2.9}$$

where $k = |\mathbf{K}^{\mu}|$. When we take $\mu = 0$, i.e. $\mu_1 = \mu_2 = 0$ so that $\mathbf{K}^{\mu} = 0$, Eq. (2.8) reduces to

$$\hat{\mathbf{q}}_0^m = \frac{\mathbf{e}^m}{\tau}. \tag{2.10}$$

Physically, the above equation states that the force acting on the fluid is balanced by the mean pressure gradient. Next, we assume $\mu \neq 0$. Taking the inner product of (2.8) with respect to $\mathbf{K}^\mu$ and substituting Eqs. (2.9) and (2.10), we obtain

$$\mathbf{K}^\mu \cdot \hat{\mathbf{q}}_\mu^m = \frac{1}{\tau} \mathbf{K}^\mu \cdot \mathbf{e}^m = \mathbf{K}^\mu \cdot \hat{\mathbf{q}}_0^m. \tag{2.11}$$

Moreover, we note that from the identity $\text{curl}(\text{ grad } q^m) = 0$, follows the equality

$$\hat{\mathbf{q}}_\mu^m \times \mathbf{K}^\mu = 0. \tag{2.12}$$

Note that the operator $\times$ in the two-dimensional space reduces to

$$\mathbf{x} \times \mathbf{y} = \begin{vmatrix} x_1 & y_1 \\ x_2 & y_2 \end{vmatrix} = x_1 y_2 - x_2 y_1.$$

From the Eqs. (2.11) and (2.12) we obtain

$$\hat{\mathbf{q}}_\mu^m = \frac{K_m^\mu}{\tau k^2} \mathbf{K}^\mu. \tag{2.13}$$

After substitution of this relation into Eq. (2.10) we find for the coefficients $\hat{\mathbf{u}}_\mu^m$,

$$\hat{\mathbf{u}}_\mu^m = \frac{1}{\tau} \left[\frac{K_m^\mu}{k^4} \mathbf{K}^\mu - \frac{1}{k^2} \mathbf{e}^m \right]. \tag{2.14}$$

From Eqs. (2.13) and (2.14), we can derive the following Fourier series for the fundamental solution in the reciprocal lattice space,

$$\begin{aligned} q^m(\mathbf{x}) &= -\frac{x_m}{\tau} + \nabla_m S_1(\mathbf{x}), \\ u_j^m(\mathbf{x}) &= u_{0_j}^m + (\delta_{jm} \Delta - \nabla_j \nabla_m) S_2(\mathbf{x}), \end{aligned} \tag{2.15}$$

where ∇_j denotes the derivative with respect to x_j and the Fourier series S_n are given by

$$S_n(\mathbf{x}) = \frac{1}{\tau} {\sum_\mu}' \frac{1}{k^{2n}} \exp(-i\,\mathbf{x} \cdot \mathbf{K}^\mu). \tag{2.16}$$

Here the prime $'$ means that the term $\mu = 0$ is excluded from the summation.

The next step will be an improvement of the convergence of the series (2.16) by applying the so-called *Ewald summation technique*. This method consists of splitting up the sum in two separate parts: one part is summed in the lattice space and the other part in the reciprocal space (cf. Nijboer and De Wette [23]). Here, we require the following identity of the *Gamma function* $\Gamma(n)$, *viz.*

$$\frac{1}{k^{2n}} = \frac{a^n}{\Gamma(n)} \int_0^\infty t^{n-1} e^{-ak^2 t}\, \mathrm{d}t = \frac{a^n}{\Gamma(n)} \int_0^1 t^{n-1} e^{-ak^2 t}\, \mathrm{d}t + \frac{\Gamma(n, ak^2)}{\Gamma(n) k^{2n}}, \tag{2.17}$$

(the first identity can be found, for example, in Abramowitz and Stegun [24, Eq. 6.1.1]). Here a is an arbitrary parameter that will be fixed below; $\Gamma(n, x)$ is the *incomplete Gamma function* which is defined by

$$\Gamma(n, x) = \int_x^\infty e^{-t} t^{n-1}\, \mathrm{d}t.$$

Substitution of the identity (2.17) in Eq. (2.16) yields

$$S_n(\mathbf{x}) = \frac{1}{\tau\Gamma(n)}{\sum_{\mu}}' \frac{\Gamma(n, ak^2)}{k^{2n}} \exp(-i\,\mathbf{x}\cdot\mathbf{K}^{\mu}) + \frac{a^n}{\tau\Gamma(n)} \int_0^1 t^{n-1}{\sum_{\mu}}' \exp(-ak^2t - i\,\mathbf{x}\cdot\mathbf{K}^{\mu})\,\mathrm{d}t. \tag{2.18}$$

The first sum on the right-hand side of the above equation converges rapidly owing to the exponential decay of the Gamma function; the convergence speed of the second sum behaves similar as the original sum (2.16). We may improve the convergence of this latter series by considering its summation in the original lattice space. In order to accomplish this, we apply the two-dimensional version of the *Poisson summation formula*, i.e.

$$\sum_{\lambda} f(\mathbf{X}^{\lambda} - \mathbf{x}) = \frac{1}{\tau}\sum_{\mu} \exp(-i\,\mathbf{x}\cdot\mathbf{K}^{\mu})\mathrm{F}(\mathbf{K}^{\mu}),$$

where $\mathrm{F}(\mathbf{k})$ is the two-dimensional Fourier transform of $f(\mathbf{x})$. Note that this summation formula can easily be deduced from the two-dimensional analogue of Parseval's theorem. In particular the following holds

$$\sum_{\lambda} \exp(-\alpha|\mathbf{x} - \mathbf{X}^{\lambda}|^2) = \frac{\pi}{\alpha\tau}\sum_{\mu} \exp\Big(-i\,\mathbf{x}\cdot\mathbf{K}^{\mu} - \frac{k^2}{4\alpha}\Big),$$

since the two-dimensional Fourier transform of the Gaussian function $\exp(-\alpha|\mathbf{x}|^2)$ is equal to $\pi\exp(-|\mathbf{k}|^2/4\alpha)/\alpha$ (see for instance Champeney [25, p.48]). Using the latter equality in the second sum of Eq. (2.18), we obtain

$$\begin{aligned}
&\int_0^1 t^{n-1}{\sum_{\mu}}' \exp(-ak^2t - i\,\mathbf{x}\cdot\mathbf{K}^{\mu})\,\mathrm{d}t \\
&\qquad = \int_0^1 t^{n-1}\sum_{\mu} \exp(-ak^2t - i\,\mathbf{x}\cdot\mathbf{K}^{\mu})\,\mathrm{d}t - \frac{1}{n} \\
&\qquad = \frac{\tau}{4\pi a}\sum_{\lambda}\int_0^1 t^{n-1}\exp\Big(-\frac{|\mathbf{x}-\mathbf{X}^{\lambda}|^2}{4at}\Big)\,\mathrm{d}t - \frac{1}{n} \\
&\qquad = \frac{\tau}{4^n a^n \pi}\sum_{\lambda} |\mathbf{x}-\mathbf{X}^{\lambda}|^{2n-2}\Gamma\Big(1-n, \frac{|\mathbf{x}-\mathbf{X}^{\lambda}|^2}{4a}\Big) - \frac{1}{n}.
\end{aligned}$$

We thus have split the Fourier series $S_n(\mathbf{x})$ in two rapidly converging sums, *viz.*

$$S_n(\mathbf{x}) = -\frac{a^n}{\tau n\Gamma(n)} + \frac{1}{4^n\pi\Gamma(n)}\sum_{\lambda} |\mathbf{x}-\mathbf{X}^{\lambda}|^{2n-2}\Gamma\Big(1-n, \frac{|\mathbf{x}-\mathbf{X}^{\lambda}|^2}{4a}\Big) + \frac{1}{\tau\Gamma(n)}{\sum_{\mu}}' \frac{\Gamma(n, ak^2)}{k^{2n}} \exp(-i\,\mathbf{x}\cdot\mathbf{K}^{\mu}), \tag{2.19}$$

whereby we observe that the parameter a can still be chosen freely. It can be shown that Eq. (2.19) is equivalent to the solution obtained by Hasimoto [20].

For deriving a workable expression for the fundamental solution (2.15), we have to evaluate $S_n(\mathbf{x})$ and it's first and/or second-order derivative with respect to $\mathbf{x}$ for n equal to 1 and 2. Note that the involved incomplete Gamma functions can be evaluated by

$$\Gamma(-1,x) = \frac{1}{x}e^{-x} - \mathrm{E}_1(x), \qquad \Gamma(0,x) = \mathrm{E}_1(x),$$
$$\Gamma(1,x) = e^{-x}, \qquad \Gamma(2,x) = (1+x)e^{-x},$$

respectively. Here $\mathrm{E}_1(x)$ denotes the *Exponential Integral*, which is defined by

$$\mathrm{E}_1(x) = \int_1^\infty e^{-xt}t^{-1}\,\mathrm{d}t.$$

After substitution of Eq. (2.19) in the fundamental solution (2.15), and working out all the derivatives, we arrive at the fundamental solution for the Stokes flow due to a lattice of unit point forces,

$$\begin{aligned} q^m(\mathbf{x}) &= -\frac{x_m}{\tau} - \frac{1}{2\pi}\sum_\lambda \frac{r_m^\lambda}{r^2}\exp\Big(-\frac{r^2}{4a}\Big) - \frac{1}{\tau}{\sum_\mu}' \frac{K_m^\mu}{k^2}\exp(-ak^2)\sin(\mathbf{x}\cdot\mathbf{K}^\mu) \\ u_j^m(\mathbf{x}) &= u_{0_j}^m - \frac{1}{8\pi}\sum_\lambda\Big[\delta_{jm}\mathrm{E}_1\Big(\frac{r^2}{4a}\Big) + 2\Big(\frac{r_j^\lambda r_m^\lambda}{r^2} - \delta_{jm}\Big)\exp\Big(-\frac{r^2}{4a}\Big)\Big] \\ &\quad + \frac{1}{\tau}{\sum_\mu}'\frac{1}{k^4}(-\delta_{jm}k^2 + K_j^\mu K_m^\mu)(1+ak^2)\exp(-ak^2)\cos(\mathbf{x}\cdot\mathbf{K}^\mu), \end{aligned} \tag{2.20}$$

where $r_j^\lambda = x_j - X_j^\lambda$ and $r = |\mathbf{x} - \mathbf{X}^\lambda|$. From the asymptotic behaviour of $\mathrm{E}_1(x)$ for x approaching zero, i.e.

$$\mathrm{E}_1(x) = -\gamma - \log x + \mathcal{O}(x) \qquad (x \to 0),$$

where $\gamma = 0.57721\,56649\ldots$ is *Euler's constant*, we observe that the fundamental solution $\mathbf{u}^m$ has a logarithmic singularity at the lattice points. Hence this solution behaves as the fundamental solution of the Stokes flow induced by a single unit point force in an infinite two-dimensional fluid, i.e. the *stokeslet*. Moreover, if we take the constant $u_{0_j}^m$ equal to

$$u_{0_j}^m = \frac{\delta_{jm}}{8\pi}\Big[\log 4a - 2 - \gamma\Big], \tag{2.21}$$

it can be shown that close to a pole the fundamental solution (2.20) reduces to a stokeslet.

From the definition of the stress tensor $\mathcal{T}_{ijm}$ for a Newtonian fluid (cf. Eq. (3.3)), we can obtain an expression for the stress in the Stokes flow induced by the lattice of unit point forces, i.e.

$$\mathcal{T}_{ijm}(\mathbf{x}) = \mathcal{T}_{ij}(q^m, \mathbf{u}^m) = -\delta_{ij}q^m + \nabla_i u_j^m + \nabla_j u_i^m.$$

Here a repeated index in an expression denotes a summation over all possible values of that index (Einstein summation convention). Substitution of the fundamental solution (2.20) and carrying out the derivatives yields

$$\mathcal{T}_{ijm}(\mathbf{x}) = \delta_{ij}\frac{x_m}{\tau} + \frac{1}{8a\pi}\sum_\lambda\Big[-\delta_{im}r_j^\lambda - \delta_{jm}r_i^\lambda + \frac{2r_i^\lambda r_j^\lambda r_m^\lambda}{r^2}\Big(1+\frac{4a}{r^2}\Big)\Big]\exp\Big(-\frac{r^2}{4a}\Big)$$

$$+\frac{1}{\tau}\sum_{\mu}{}'\frac{1}{k^4}\Big[\Big(1+ak^2\Big)\Big(k^2(\delta_{im}K_j^\mu+\delta_{jm}K_i^\mu)\;-\;2K_i^\mu K_j^\mu K_m^\mu\Big)$$

$$+\;\delta_{ij}k^2K_m^\mu\Big]\exp(-ak^2)\sin(\mathbf{x}\cdot\mathbf{K}^\mu). \tag{2.22}$$

Finally, we have to fix the parameter a which controls the convergence speed of the two lattice sums in the original and the reciprocal space. Ideally, this parameter has to be taken such that both series are converging at equal rates. This can be accomplished by requiring the same exponential decay in both lattice sums, which yields the following value for the convergence parameter a, *viz.*

$$a\;=\;\frac{|\tau|}{4\pi}. \tag{2.23}$$

Note that this value is the two-dimensional analogue of the convergence parameter which is used in the case of a lattice sum in three-dimensional space (cf. Beenaker [26]).

In the derivation of the integral formulation, as we will outline in the section below, we also require the fundamental solution due to a lattice of point sources. This fundamental solution, say $\tilde{\mathbf{u}}$ and $\tilde{q}$, satisfies the following equations

$$\Delta\,\tilde{\mathbf{u}}\;-\;\operatorname{grad}\tilde{q}\;=\;0;\qquad\qquad \operatorname{div}\tilde{\mathbf{u}}\;=\;-\sum_{\lambda}\delta(\mathbf{x}-\mathbf{X}^\lambda). \tag{2.24}$$

The solution of the above equations can be obtained by assuming that

$$\tilde{\mathbf{u}}\;=\;\operatorname{grad}\varphi. \tag{2.25}$$

Substitution of this relation in both the equations of (2.24) yields

$$\operatorname{grad}\tilde{q}\;=\;\operatorname{grad}\,\Delta\,\varphi;\qquad\qquad \Delta\varphi\;=\;-\sum_{\lambda}\delta(\mathbf{x}-\mathbf{X}^\lambda). \tag{2.26}$$

Using the equality

$$\Delta S_1(\mathbf{x})\;=\;-\sum_{\lambda}\delta(\mathbf{x}-\mathbf{X}^\lambda)\;+\;\frac{1}{\tau},$$

we find

$$\varphi(\mathbf{x})\;=\;-\frac{|\mathbf{x}|^2}{4\tau}\;+\;S_1(\mathbf{x}). \tag{2.27}$$

Next, from the Eqs. (2.26), (2.27), (2.19) and (2.23) we derive the following series for the fundamental solution

$$\tilde{q}(\mathbf{x})\;=\;-\sum_{\lambda}\delta(\mathbf{x}-\mathbf{X}^\lambda)\;=\;0, \tag{2.28}$$

$$\begin{aligned}\tilde{u}_j(\mathbf{x})\;&=\;-\frac{x_j}{2\tau}\;+\;\nabla_j S_1(\mathbf{x})\\ &=\;-\frac{x_j}{2\tau}-\frac{1}{2\pi}\sum_{\lambda}\frac{r_j^\lambda}{r^2}\exp\Big(-\frac{\pi r^2}{\tau}\Big)-\frac{1}{\tau}\sum_{\mu}{}'\frac{K_j^\mu}{k^2}\exp\Big(-\frac{\tau k^2}{4\pi}\Big)\sin(\mathbf{x}\cdot\mathbf{K}^\mu).\end{aligned} \tag{2.29}$$

Note that $\tilde{q} = 0$ follows from the fact that $\mathbf{x} \neq \mathbf{X}^\lambda$, since a lattice of point sources is required which are situated inside the interior of each hole in a cell (cf. Van de Vorst [14]).

For the fundamental stress tensor $\tilde{T}$, using the above equation, we find

$$\tilde{T}_{ij}(\mathbf{x}) = -\frac{\delta_{ij}}{\tau} - \frac{1}{\pi}\sum_{\lambda}\left(\delta_{ij} - 2r_i^\lambda r_j^\lambda\left(\frac{1}{r^2} + \frac{\pi}{\tau}\right)\right)\frac{1}{r^2}\exp\left(-\frac{\pi r^2}{\tau}\right) - \frac{2}{\tau}{\sum_{\mu}}'\frac{K_i^\mu K_j^\mu}{k^2}\exp\left(-\frac{\tau k^2}{4\pi}\right)\cos(\mathbf{x}\cdot\mathbf{K}^\mu). \tag{2.30}$$

3. Integral formulation for the unit cell

Here, we will deduce an integral formulation for the unit cell of a two-dimensional lattice by applying the fundamental solutions which were derived in the previous section. However, before we outline this derivation, we will briefly summarize the governing equations which describe the viscous sintering phenomenon.

Here we assume that the sintering gel can be represented by a periodic continuation, in two directions, of a unit cell at *any stage* during the densification process. Hence the shrinkage of the unit cell corresponds to the shrinkage rate of the whole gel in the two-dimensional plane. The material transport by viscous sintering is modelled as a viscous incompressible Newtonian fluid driven solely by surface tension, cf. Kuiken [1]. Therefore, the Stokes creeping flow equations are valid, which can be characterized by the *dynamic viscosity* η, the *surface tension* γ and the magnitude of the body say through its *cross-section*, i.e. length ℓ. We define a characteristic velocity v_c, a characteristic pressure p_c and a characteristic time t_c based on the parameters γ, η and ℓ by

$$v_c = \frac{\gamma}{\eta}, \qquad p_c = \frac{\gamma}{\ell}, \qquad t_c = \frac{\ell\eta}{\gamma}.$$

Using these characteristic parameters and taking ℓ as the characteristic length, we obtain for the Stokes equation the following dimensionless form

$$\Delta\mathbf{v} - \operatorname{grad} p = 0. \tag{3.1}$$

Here $\mathbf{v}$ denotes the dimensionless velocity and p is the dimensionless pressure of the flow. The conservation of mass can be expressed by the continuity equation

$$\operatorname{div}\mathbf{v} = 0. \tag{3.2}$$

The dimensionless stress tensor $\mathcal{T}$ for a Newtonian fluid is defined by

$$\mathcal{T}_{ij} = -p\delta_{ij} + \left(\frac{\partial v_i}{\partial x_j} + \frac{\partial v_j}{\partial x_i}\right). \tag{3.3}$$

On the boundary, the dimensionless tension in the normal direction, say $\mathbf{b}$, for a free fluid surface can be found as (Batchelor [27, p.150])

$$b_i := \mathcal{T}_{ij}n_j = -\kappa n_i, \tag{3.4}$$

where κ is the curvatures of the boundary and $\mathbf{n}$ is the outward unit normal vector.

The motion of the boundary is obtained by applying the Lagrangian representation for the boundary velocity $\mathbf{v}$,

$$\frac{\mathrm{d}\mathbf{x}}{\mathrm{d}t} = \mathbf{v}(\mathbf{x}), \qquad (\mathbf{x} \in \Gamma), \tag{3.5}$$

where t is the dimensionless time. The above kinematic constraint expresses the displacement of the material boundary particles: the trajectories of those particles are followed. Hence a *quasi-static* approach is used to solve the viscous sintering problem.

For the derivation of an integral formulation for the boundary velocity of a particular unit cell, we require the so-called *Green's formula* corresponding to the Stokes problem, i.e.

$$\int_\Omega \left[\left(\Delta v_i - \frac{\partial p}{\partial x_i} \right) u_i - \left(\Delta u_i + \frac{\partial q}{\partial x_i} \right) v_i \right] \mathrm{d}\Omega = \\ = \int_\Gamma \left[\mathcal{T}_{ij}(p, \mathbf{v}) u_i n_j - \mathcal{T}_{ij}(-q, \mathbf{u}) v_i n_j \right] \mathrm{d}\Gamma, \tag{3.6}$$

where Ω denotes a closed fluid domain that is surrounded by a boundary denoted by Γ. Here Γ represents the union of both the outer boundary of the unit cell, say Γ_0, and the boundaries of the pores in the inside of the cell which are denoted by Γ_k (k=1,..,M). The above integral identity can easily be derived by the integration over Ω of the derivative of the stress tensor together with the application of the divergence theorem of Gauss.

Moreover, we note that if the vector $\mathbf{x}$ in the fundamental solution (2.20) is replaced by $\mathbf{x} - \mathbf{y}$, the obtained functions $\mathbf{u}^m(\mathbf{x} - \mathbf{y})$ and $q^m(\mathbf{x} - \mathbf{y})$ are still the solutions of the Stokes problem (2.2). It can also be verified that these functions are the solutions to the *adjoint system*, i.e.

$$\Delta_y \mathbf{u}^m(\mathbf{x}, \mathbf{y}) + \mathrm{grad}_y q^m(\mathbf{x}, \mathbf{y}) = \sum_\lambda \delta(\mathbf{x} - \mathbf{y} - \mathbf{X}^\lambda) \mathbf{e}^m, \\ \mathrm{div}_y \mathbf{u}^m = 0. \tag{3.7}$$

By $(\,)_y$ we mean that the differentiation is carried out with respect to $\mathbf{y}$.

We replace $\mathbf{u}$ and q in Green's formula (3.6) with the fundamental singular solutions $\mathbf{u}^m(\mathbf{x} - \mathbf{y})$, $q^m(\mathbf{x} - \mathbf{y})$ and consider these as function of $\mathbf{y}$, thus constituting the solution of the adjoint system (3.7). Furthermore, the domain Ω is taken equal to a unit cell and we require that $\mathbf{v}$ and p satisfy the Stokes problem (3.1) and (3.2). Then we obtain the following *Fredholm integral equation of the second kind*,

$$v_m(\mathbf{x}) = \int_\Gamma \mathcal{T}_{ij}(-q^m, \mathbf{u}^m)_y v_i n_j \, \mathrm{d}\Gamma_y - \int_\Gamma \mathcal{T}_{ij}(p, \mathbf{v}) u_{mi} n_j \, \mathrm{d}\Gamma_y, \tag{3.8}$$

for *any* $\mathbf{x} \in \Omega$. Here the coefficient $u_{mi} = u_i^m(\mathbf{x} - \mathbf{y})$, i.e. Eq. (2.20). The vector $\mathcal{T}_{ij}(p, \mathbf{v}) n_j$ is given by the boundary condition (3.4), i.e. $\mathcal{T}(p, \mathbf{v})\mathbf{n} = \mathbf{b}$. Moreover, it can be seen that for the other kernel, say q_{mi}, holds

$$q_{mi}(\mathbf{x} - \mathbf{y}) = \mathcal{T}_{ij}(-q^m, \mathbf{u}^m)_y \, n_j = -\mathcal{T}_{ij}(q^m, \mathbf{u}^m)_x \, n_j = -\mathcal{T}_{ijm}(\mathbf{x} - \mathbf{y}) \, n_j.$$

Thus, using Eq. (2.22) and the optimal choice for the parameter a, *viz.* Eq. (2.23), we obtain for $q_{mi}(\mathbf{x})$ the following expression,

$$q_{mi}(\mathbf{x}) = \frac{1}{2|\tau|} \sum_\lambda \left[-r_i^\lambda n_m - \delta_{mi} r_j^\lambda n_j + \frac{2 r_m^\lambda r_i^\lambda r_j^\lambda n_j}{r^2} \left(1 + \frac{|\tau|}{\pi r^2} \right) \right] \exp\left(- \frac{\pi r^2}{|\tau|} \right)$$

$$+\frac{1}{\tau}\sum_{\mu}{}'\frac{1}{k^4}\left[\left(1+\frac{|\tau|k^2}{4\pi}\right)\left(k^2(K_i^\mu n_m-\delta_{mi}K_j^\mu n_j)-2K_m^\mu K_i^\mu K_j^\mu n_j\right)\right.$$

$$\left.+\,k^2K_m^\mu n_i\right]\exp\left(-\frac{|\tau|k^2}{4\pi}\right)\sin(\mathbf{x}\cdot\mathbf{K}^\mu)+\frac{x_m n_i}{\tau}. \tag{3.9}$$

When we let $\mathbf{x}$ in Eq. (3.8) approach the boundary and use the assumption that this boundary is "smooth", we arrive at the following integral formulation

$$\tfrac{1}{2}v_j(\mathbf{x})+\int_\Gamma q_{ij}(\mathbf{x}-\mathbf{y})v_j(\mathbf{y})\,\mathrm{d}\Gamma_y=\int_\Gamma u_{ij}(\mathbf{x}-\mathbf{y})b_j(\mathbf{y})\,\mathrm{d}\Gamma_y, \tag{3.10}$$

where the kernels u_{ij} and q_{ij} are given by the Eqs. (2.20) and (3.9), respectively.

As in the two-dimensional formulation, when we used a stokeslet as a fundamental solution (cf. Van de Vorst [14, 2]), we have to deflate the above integral Eq. (3.10) with respect to the outward normal in order to make the integral equation uniquely defined and to accomplish that the pores in the inside of the unit cell are vanishing.

Here we will only give the resulting integral formulation after the deflation is accomplished. Therefore, we require the integral equation in which the fundamental solution for a point force is used, for this deflation with respect to the outward normal. Substitution of Eqs. (2.29) and (2.30) in the Green's formulae (3.6) yields

$$\int_\Gamma \tilde{q}_i(\mathbf{x}-\mathbf{y})v_i(\mathbf{y})\,\mathrm{d}\Gamma_y=\int_\Gamma \tilde{u}_i(\mathbf{x}-\mathbf{y})b_i(\mathbf{y})\,\mathrm{d}\Gamma_y,$$

where

$$\tilde{q}_i(\mathbf{x}-\mathbf{y})=\tilde{T}_{ij}(\mathbf{x}-\mathbf{y})\,n_j,$$

and in all the holes we choose an *arbitrary* point: let $\mathbf{z}^m$ be a point in the inside of the area surrounded by Γ_m (m=1,...,M).

Then the *deflated* formulation of integral Eq. (3.10) can be expressed as,

$$\frac{1}{2}v_i^m(\mathbf{x}^m)+\sum_{k=0}^{M}\int_{\Gamma_k}q_{ij}(\mathbf{x}^m-\mathbf{y})v_j^k\,\mathrm{d}\Gamma_y+(1-\delta_{0m})n_i^m(\mathbf{x}^m)\int_{\Gamma_m}\tilde{q}_j(\mathbf{z}^m-\mathbf{y})v_j^m\,\mathrm{d}\Gamma$$

$$=\sum_{k=1}^{M}\int_{\Gamma_k}u_{ij}(\mathbf{x}^m-\mathbf{y})b_j^k\,\mathrm{d}\Gamma_y+(1-\delta_{0m})n_i^m(\mathbf{x}^m)\int_{\Gamma_m}\tilde{u}_j(\mathbf{z}^m-\mathbf{y})b_j^m\,\mathrm{d}\Gamma. \tag{3.11}$$

Here the superscript ^{m} denotes that the particular variable is lying on the boundary of hole Γ_m. Note that the contribution of the cell boundary Γ_0 for the right-hand side is not included, since it can be shown that this particular integral is equal to zero for *every arbitrary periodic force* **b**. This is a very nice property, because we cannot give an expression for the force on the outer boundary anyway. The above integral formulation is applied to simulate the densification of the unit cell in the Stokes flow with vanishing holes in the inside.

4. Numerical solution

The integral Eq. (3.11) is solved by applying a BEM. Hence the boundary is discretized into a set of N nodal points; the boundary curve Γ is replaced by a polygon through these

nodal points. Moreover, the integral formulation is enforced on the polygon for each of the collocation points. This results in a square full rank system of 2N linear algebraic equations with 2N unknowns which will be denoted by,

$$\mathcal{H}(x)\, v \;=\; \mathcal{G}(x)\, b(x), \tag{4.1}$$

where x is a vector of length 2N that consists of all successive collocation points, *viz.*

$$x \;=\; \left[x_1^1, x_2^1, x_1^1, x_2^1, ..., x_1^N, x_2^N\right]^T,$$

whereas the vectors v and b represent the corresponding boundary velocity and tension respectively. The vector b is known (cf. Eq. (3.4)): this vector is approximated by fitting a quadratic polynomial through three successive collocation points. The unknowns v are obtained after solving the linear square full rank system (4.1) by Gaussian elimination with partial pivoting (LU-decomposition). More details about the implementation of the BEM for general Stokes-flow problems can be found, for example, in Van de Vorst [2].

However, an extra detail in the present formulation is the accurate calculation of the lattice and reciprocal lattice summations which occur in the kernels of the integral Eq. (3.11). Because of the exponential decay of the separate terms in the lattice sums, we observed that summation over two or three lattice and reciprocal lattice layers was enough to obtain sufficient accuracy.

A point of concern is that the basic vectors $\mathbf{a}^i$ of the cell are varying, due to the densification of the lattice cell as time proceeds. Using the velocity of the corners of the outer cell boundary, these basic vectors can be calculated at each time step. Note that owing the periodicity of the cell corner velocities, it is sufficient to compute only one corner velocity. Hence the discretized system of unknowns which is obtained from the outer cell boundary Γ_0, can be reduced to two unknowns: the velocity in the 1- and 2-direction.

After calculating the required velocity field, we have to perform a time step. Using the kinematic constraint (3.5) for each collocation point together with Eq. (4.1), we obtain the following 2N non-linear system of ODEs,

$$\frac{\mathrm{d}x}{\mathrm{d}t} \;=\; \mathcal{H}^{-1}(x)\, \mathcal{G}(x)\, b(x). \tag{4.2}$$

In the available literature about free creeping Stokes flows this system of ODEs is discretized by a simple forward Euler scheme or other explicit schemes. However, it appears that the above system of ODEs can be *stiff* for certain type of shapes (*e.g.* shapes which have cusp-like regions); then the time step in the forward Euler scheme has to be taken very small to obtain a stable method. Therefore, we have implemented a variable-step, variable-order Backward-Differences-Formulae (BDF) method to solve these ODEs. More details about this implementation are available in Van de Vorst and Mattheij [15].

The collocation points of the boundary are (re)distributed after a certain number of time steps. In Van de Vorst and Mattheij [13], we proposed an algorithm for a fairly optimal node redistribution based on equidistributing the curvature of the boundary. The aim of that algorithm is twofold. Firstly, the number and position of the discretization points are optimized, which is important because the computational costs per time step are proportional to $(2N)^3$. Secondly, the algorithm treats regions with a large curvature "cusp" such that the curvature of this particular region is preserved after redistribution to avoid (numerical) oscillations in the computed velocity field.

5. Numerical results

Results of numerical simulation for a number of two-dimensional sintering geometries are presented to demonstrate the correctness of the mathematical formulation developed and to show some typical evolution properties.

5.1. Validation of mathematical model

We will investigate the influence of the choice of the unit cell in a fluid with both uniformly sized and distributed pores, on the numerically obtained densification results of this geometry. In order to validate the mathematical formulation as outlined in the previous sections, the differences in densification rates have to be minimal with respect to the choice of the representative unit cell.

Therefore we consider a fluid with cylindrical pores of radius 0.5 which are distributed uniformly in the two-dimensional plane. The distance between the centers of two subsequent pores is taken equal to 2. A part of this fluid domain is shown in Fig. 2. We consider the densification of this fluid domain for three different choices of unit cells as indicated in the same picture (**a–c**). Hence the unit cells consist of 1, 4 or 9 cylindrical pores. The shape deformation of the various unit cells is also plotted in Fig. 2 at subsequent time steps $t = 0.0(0.1)1.0$.

The density, say ρ, of the fluid domain at a particular time is found from dividing of the surface occupied by fluid in the unit cell by the total area that surrounds the outer boundary of the cell. In Fig. 3 the numerically obtained densification rate is plotted for the three cells as time evolves. From this plot, we observe that the differences between the three shrinkage rates are very small: this gives some validation of our proposed mathematical approach. Hence, we can restrict ourself to consider the densification of the most simple unit cell, i.e. **a**. Note that from the figure it can be observed that the densification proceeds at an almost linear rate here. We have also plotted the densification rates resulting from the analytical models of both Mackenzie and Shuttleworth [18] (*closed-pores model* or *MS-model*) and Scherer [19] (*open-pores model*).

The model of Mackenzie and Shuttleworth [18] is generally used to describe the late-stage viscous sintering of the gel. The densification results from the shrinkage of spherical pores distributed uniformly throughout the fluid. Moreover, it is assumed that all the pores have an identical radius. The closed-pores model in full dimensional variables gives the following analytical relationship between the relative density of the sintering gel and the reduced time,

$$K_3(t - t_0) = \tfrac{2}{3}\left(\tfrac{3}{4\pi}\right)^{\frac{1}{3}}\left(\tfrac{1}{2}\log\left[\frac{(1+a_0)^3(1+a^3)}{(1+a)^3(1+a_0^3)}\right] + \sqrt{3}\arctan\left[\frac{2\sqrt{3}(a_0 - a)}{3 + (2a_0 - 1)(2a - 1)}\right]\right), \tag{5.1}$$

where

$$K_3 = \frac{\gamma n^{\frac{1}{3}}}{\eta}; \qquad a(\hat{\rho}) = \left(\frac{1-\hat{\rho}}{\hat{\rho}}\right)^{\frac{1}{3}}; \qquad a_0 = a(\hat{\rho}_0); \qquad \hat{\rho}_0 = \frac{\rho_0}{\rho_s}; \quad \text{and} \quad \hat{\rho} = \frac{\rho}{\rho_s},$$

with $0 < \hat{\rho}_0 \leq \hat{\rho} < 1$. Here ρ is the bulk density of the gel, ρ_0 is the initial bulk density (at $t = t_0$), ρ_s is the density of the solid phase (skeletal density) and n is the number of closed pores per unit of volume of solid phase.

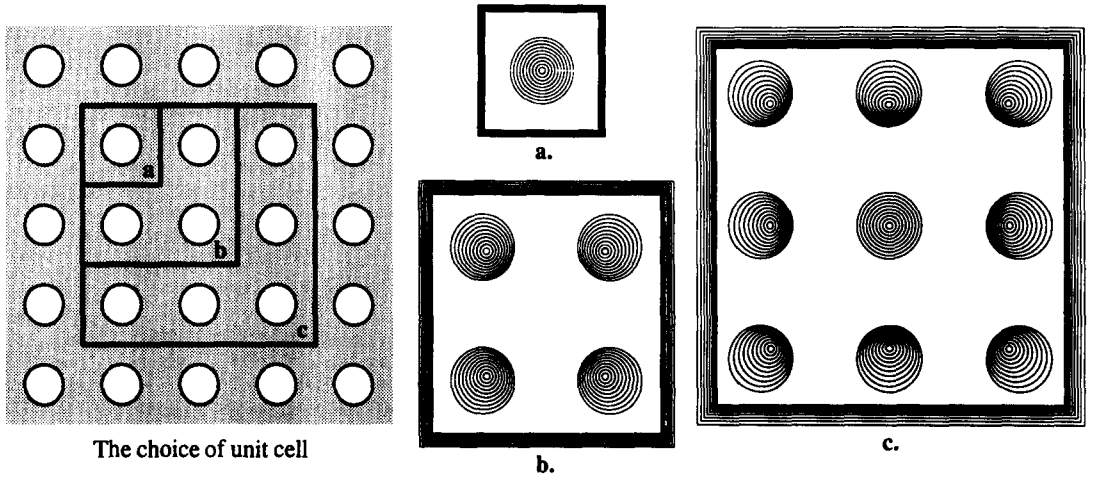

Fig. 2. Some choices of unit cells that can be made in a Stokes flow with uniformly sized and distributed cylindrical pores. In (a)–(c) is shown the densification shapes of the various unit cells at three subsequent time steps.

In the two-dimensional plane, we can deduce an analogous closed pores model by assuming that the densification results from the shrinkage of uniform cylindrical pores distributed throughout the fluid. The following densification rate is then obtained

$$K_2(t - t_0) = \frac{1}{\sqrt{\pi}}\left[\arcsin(1 - \hat{\rho}_0) - \arcsin(1 - \hat{\rho})\right], \tag{5.2}$$

where $K_2 = \gamma\sqrt{n}/\eta$. In the sequel, we will refer to (5.1) as the 3D closed pores model and to (5.2) as the 2D closed pores model.

The so-called *open-pores model* of Scherer [19] is normally used to analyze the early and intermediate stage of the sintering process. As was stated in the introduction, in this description it is assumed that the gel can be modelled as a regular three-dimensional array of interconnected liquid cylinders. For the unit cell representing this structure, a cubic is taken which is characterized by the edge length and the cylinder radius. After approximating the flow field of this unit cell, the following densification equation can be deduced

$$K_3(t - t_0) = \frac{1}{2^{\frac{1}{6}}}\left(\tfrac{1}{2}\log\left[\frac{(1 - b_0 + b_0^2)(1 + b)^2}{(1 - b + b^2)(1 + b_0)^2}\right] + \sqrt{3}\arctan\left[\frac{2\sqrt{3}(b_0 - b)}{3 + (2b_0 - 1)(2b - 1)}\right]\right), \tag{5.3}$$

where

$$b = \left(\frac{2(1 + \cos\tfrac{1}{3}\varphi)}{1 - 2\cos\tfrac{1}{3}\varphi}\right)^{\frac{1}{3}}; \qquad \varphi = \arctan\left[\frac{8\sqrt{2\hat{\rho}(\pi^3 - 32\hat{\rho})}}{\pi^3 - 64\hat{\rho}}\right] + \begin{cases} \pi & \hat{\rho} < \pi^3/64 \\ 2\pi & \hat{\rho} > \pi^3/64, \end{cases}$$

and b_0 is found by substituting φ_0 in the relation for b. The variable φ_0 is similarly defined by using $\hat{\rho}_0$ instead of $\hat{\rho}$ in the equation above. Eq. (5.3) applies for $0 \leq \hat{\rho} \leq 0.942$ only, since it can be shown that at the density $\hat{\rho} = 0.942$ the parallel cylinders of the unit cell touch. Next, each cell contains an isolated pore so that the closed pores model applies.

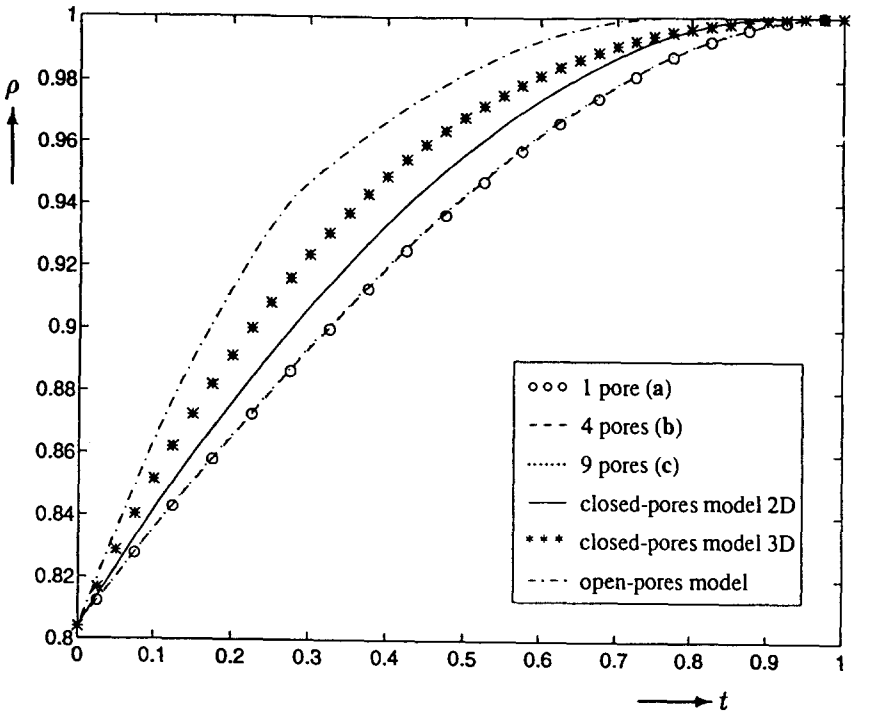

Fig. 3. A good matching is obtained when we compare the numerically obtained density (ρ) changes of the three unit cells of figure 2 as time (t) proceeds. Both the analytic relations of the open- and closed-pores model predict an almost similar behaviour of the shrinkage rate.

The dimensionless form of the analytical densification Eqs. (5.1)–(5.3) can easily be found by skipping the factor γ/η and taking $\rho_s = 1$, hence $\hat{\rho} = \rho$. Moreover, we note that in the above three models the pores are assumed to be of equal size and distributed uniformly throughout the sintering material. Although the Eqs. (5.1) and (5.3) are developed for a really three-dimensional sintering gel, the comparison with the numerical results gives some quantitative insight in the reliability and limitations of those approximations. When comparing these analytical predictions with the densification rate obtained numerically, as is shown in Fig. 3, we observe that during the initial stage the numerical shrinkage rate proceeds slightly more slowly than the analytical predictions; the opposite holds during the later stages of the densification. Moreover, we observe a reasonable agreement between the numerical results and the closed pores model in two dimensions, i.e. relation (5.2). The latter observation also provides some justification for the mathematical model proposed in this paper.

A more complicated densification problem is the sintering of a regular packing of equally sized cylinders. A part of this packing is shown in Fig. 4. The initial radii of all cylinders is taken equal to 0.5 and the contact radius, say r, between two touching cylinders, the so-called *neck region*, is initially set equal to 0.095 for all the coalescing regions. Furthermore, we use Hopper's analytical solution for the coalescence of two equal cylinders to approximate the neck regions of the initial shape (cf. Hopper [5]). In Figs. 4a–4c we show the densification of these three unit cells. All curves are plotted at equal periods of 0.1. An explanation for the differences in shape deformation of these three cells can be found from the mathematical formulation itself, i.e. the evolution differences are not due to numerical errors. Since the basic lattice vectors are taken equal to the outer boundary of all the three cells, the periodicity

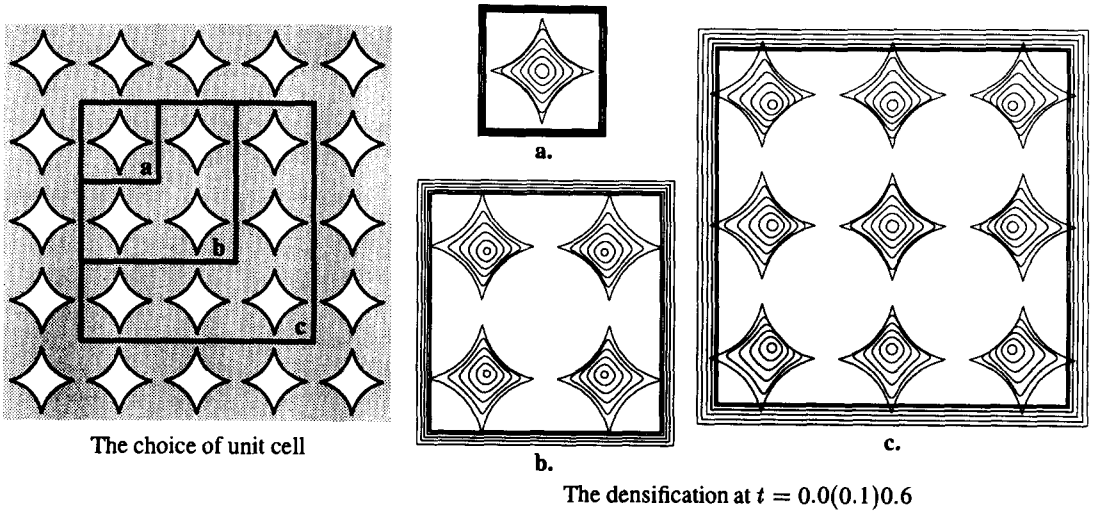

Fig. 4. The choice of unit cell that can be made in a Stokes flow with uniformly sized and distributed cylindrical particles. In (**a**)–(**c**) is shown the densification shape of the various unit cells at subsequent time steps.

of the velocity field is imposed on these cell boundaries. Therefore, in the case of the 4 and 9 pores cells these pores have the freedom to approach one another. However, this translation of pores should not have any effect on the various densification rates. Therefore, a comparison of the numerically obtained densification rates is shown in Fig. 5. Now we observe that the differences are larger between these three curves, compared with the numerical results obtained in the previous example. However, the general behaviour of the three curves is similar, so that we may still conclude that our mathematical formulation holds.

In Fig. 5 we have also compared the densification rate of the above mentioned unit cells to the analytical open and closed-pores models. Now we observe that these relations predict quite a different densification evolution during the early stages as compared with the obtained numerical simulation results: the numerically obtained rate proceeds much slower than the analytical predictions. This is caused by a smoothing of the neck region during this stage, which results in only a small reduction of the pore size. Hence this example illustrates that the densification rate depends on the pore shape of the initial geometry.

An interesting question is the behaviour of the neck growth between two touching cylinders of these packings compared to the exact contact radius development of two coalescing cylinders. In Fig. 6 we show the development in time of the contact radius for the unit cell 4a. The exact neck radius for the coalescence of two cylinders with initial radii equal to 0.5, as obtained from Hopper's analytical solution, is also plotted. From this picture we see that only during the initial stage the neck growth is similar to the contact radius development of two coalescing cylinders, i.e. during the smoothening of the neck region. Thereafter, the contact radius is increasing much slower in comparison with the analytic solution. Hence the latter prediction should only be used during the early stage of the sintering process.

5.2. Densification effects due to irregularities

In practice, one does not deal with a uniform-size pore distribution or a regular packed array of cylinders as we considered in the above subsection. Usually, the sintering compact is an irregular particle packing that consists of a variety of particle sizes with (often) a non-

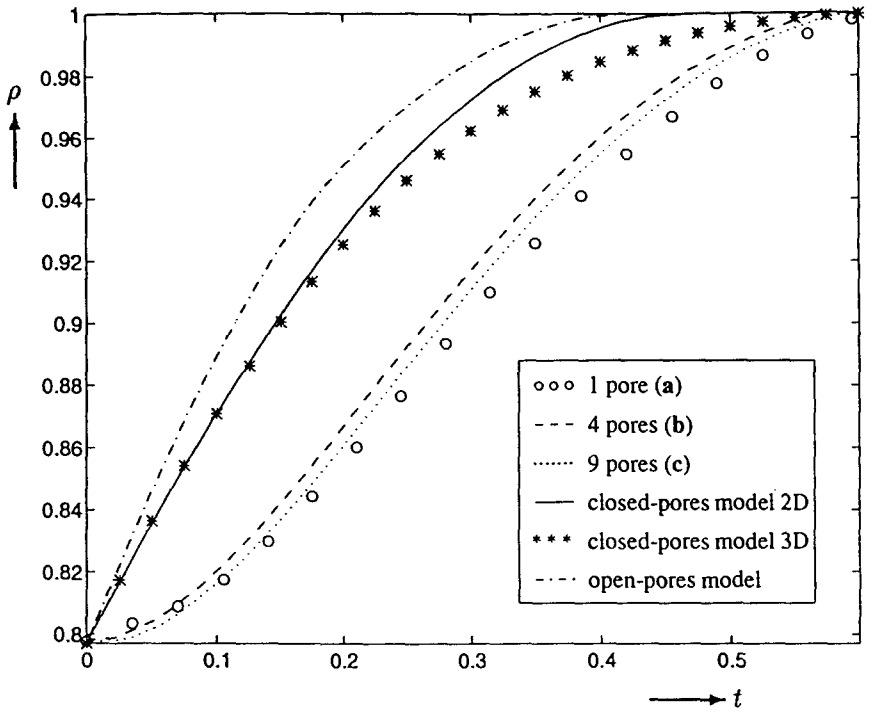

Fig. 5. A sufficient matching is obtained when we compare the densification rates of the above three unit cells. During the early stage the numerical densification behaviour differs considerably with the prediction of the analytic open and closed pores models.

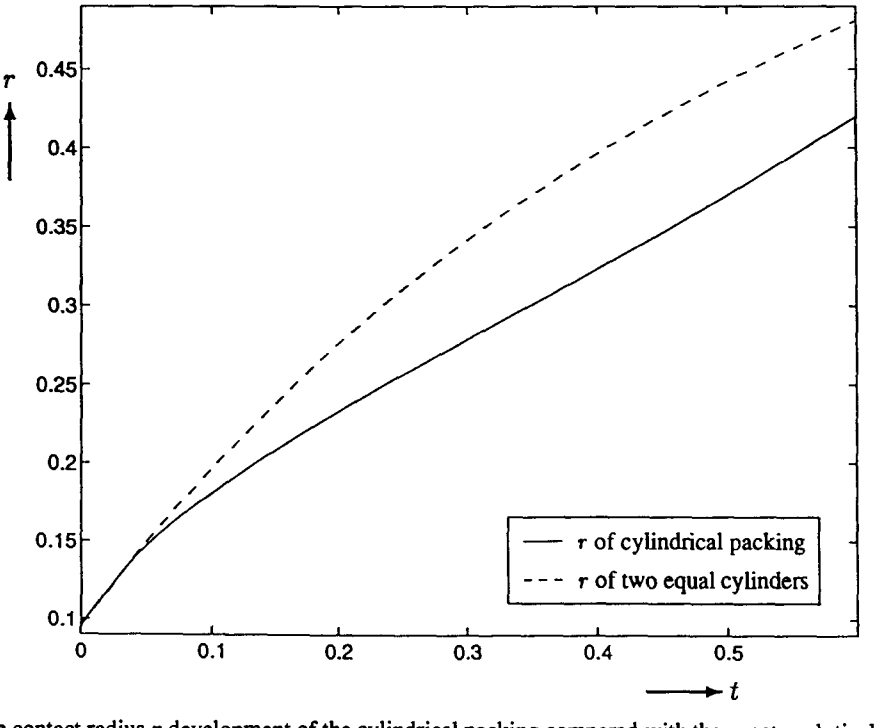

Fig. 6. The contact radius r development of the cylindrical packing compared with the exact analytical solution of the coalescence of two equal cylinders shows only an agreement during the early stages. At later time stages, the neck radius of the cylindrical packing develops much more slowly.

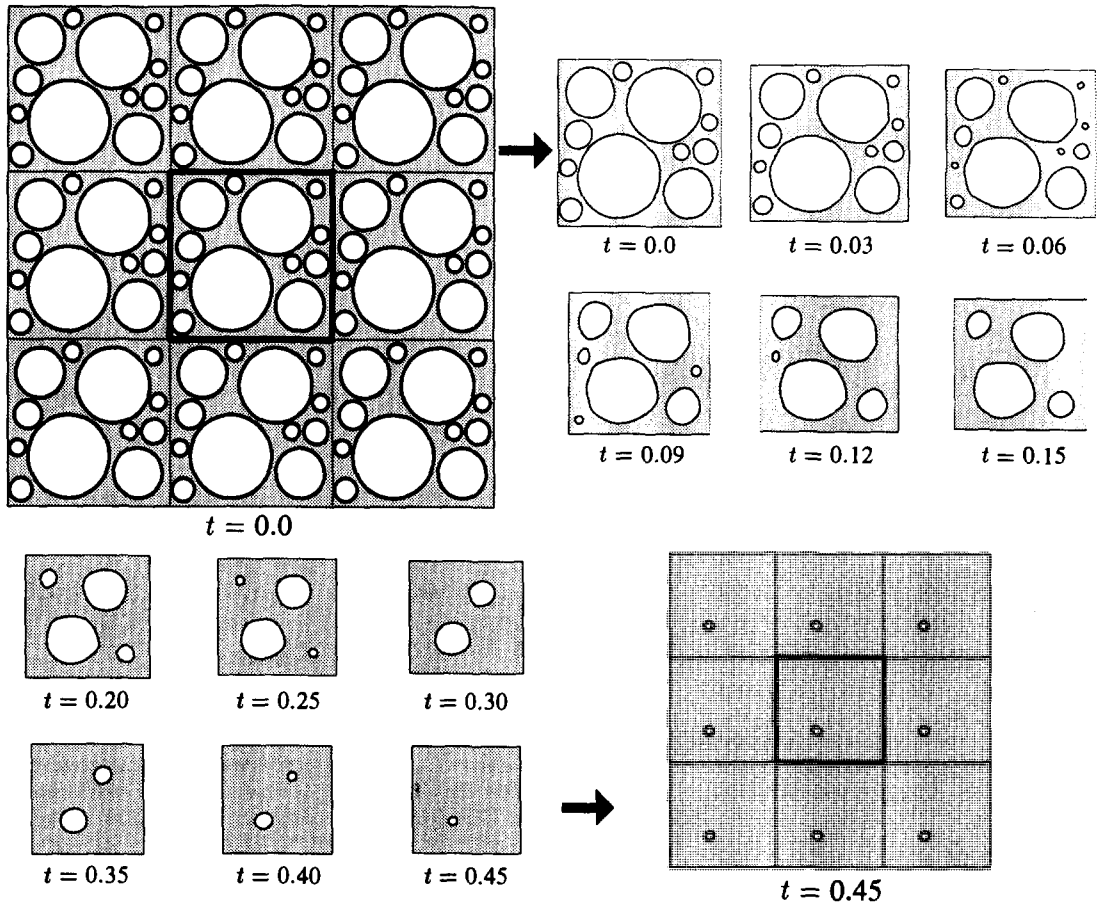

Fig. 7. The shape deformation of the unit cell of a periodic lattice of non-uniformly sized cylindrical pores at subsequent times shows that the pores vanish in order of size.

spherical–(cylindrical) form. Moreover another effect due to these irregularities has to be taken into account: the rearrangement of particles and the opening and closure of pores induced by this rearranging of particles.

Because of this, an important issue in sintering research is the quantification of the rest-porosity of the gel after sintering. The scientific interest for this densification process is to understand the magnitude of the driving force for this process and to deduce how the driving force and thus the densification rate are affected by the gel microstructure as is illustrated by the last example of the previous subsection.

The effect of nonuniformly sized and distributed pores can be illustrated by the fluid lattice plotted in Fig. 7 at $t = 0.0$. Here we consider a unit cell of length 1 by 1 with 12 nonuniformly sized cylindrical pores from which the radii are varying between 0.05 and 0.25. The plots at various time steps of the deformed cell shape show that the pores vanish in the order of their sizes one after the other: all pores are shrinking, which results in the vanishing of the smallest pores first, followed by the larger pores. Moreover, we observe from these pictures that the aspect ratio of the unit cell is changing, which might be seen as an effect on the shrinkage of the entire viscous sintering body.

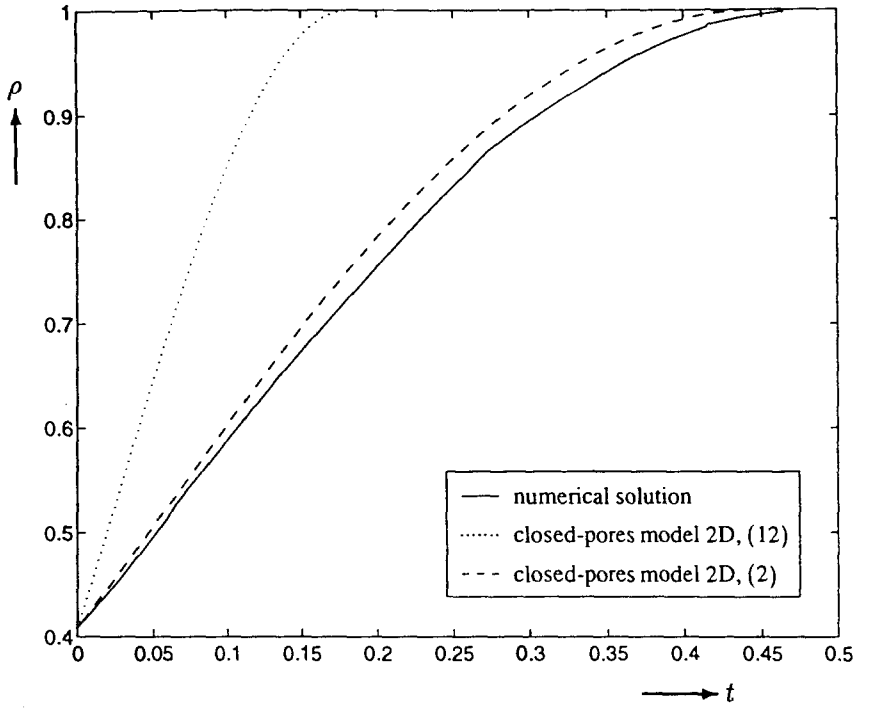

Fig. 8. The numerical densification rate of the periodic lattice of nonuniformly sized cylindrical pores of figure 7 is compared with the two-dimensional closed pores model prediction. A good matching is obtained when in this model only the significantly largest pores of the unit cell are taken (2) compared to the case when all the pores are counted (12).

This behaviour is the opposite of the numerical results obtained for a *finite* two-dimensional fluid region with nonuniform sized pores (cf. Van de Vorst [2, p.117]). There, it appears that the initially larger sized pores are shrinking significantly faster as compared to the smallest ones as time evolves. This difference can be explained from the fact that in the finite domain case, the fluid obtains an extra tension due to the curvature of the outer boundary.

In Fig. 8 the numerically obtained densification rate of the above unit cell is plotted, which is compared with the two-dimensional closed-pores model prediction (5.2). A good matching is obtained in this model when the significantly largest pores of the unit cell are counted only ($n = 2/0.409$), i.e. the smaller pores are ignored. When all pores are taken into account ($n = 12/0.409$), the predicted densification rate decreases considerably.

All pores in the cells we considered so far were shrinking during the entire densification process. However, it might also be possible that some pores first grow in size, before they shrink and vanish. This process will influence the densification rate negatively. In Fig. 9 this phenomenon is demonstrated. The unit cell represents a texture model of an aerogel that is formed in a base-catalysed way (after Craievich *et al.* [28]). Initially, the size of the rectangular unit cell is taken as 2.1 by 2.8, with density $\rho_0 = 0.439$ and it contains 17 pores.

Again it can be seen from the subsequent time plots in Fig. 9 that the smaller pores vanish first. Moreover, we observe that during the early time stages some pores become larger in size before they start shrinking. Especially, this occurs for pores that have large *concave* boundary parts. Such pores have much longer boundary lengths than what would strictly be required to surround the pore contents. Hence such pores may expand, whereas the total pore boundary

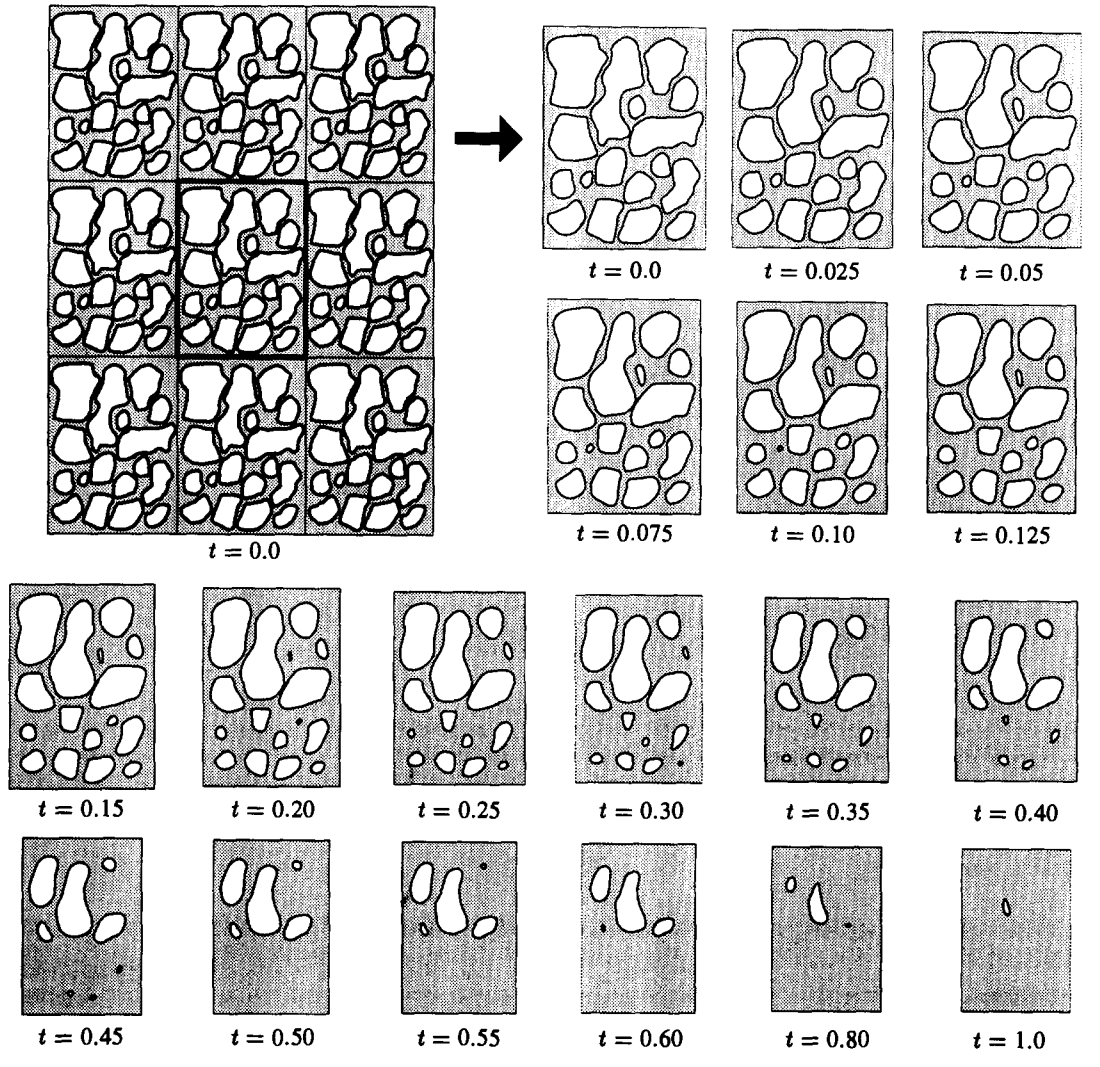

Fig. 9. The densification of a texture model of a base-catalysed aerogel demonstrates that some pores are growing initially before they start shrinking. This phenomenon influences the densfication rate negatively.

length still decreases as time evolves. Thus we conclude that one should avoid such kind of pore shape as much as possible.

The density change of the unit cell of the aerogel texture model is plotted by a solid line in Fig. 10 for increasing time. In the same figure we have also plotted the results obtained from the analytical closed-pores model prediction. Again, we observe that this equation provides the most accurate prediction of the numerical densification rate when only the three largest pores are counted in the densification relation (n=3/2.579). However, the predicted densification rate deviates more from the numerical solution which is caused by the pore growing phenomenon. It appears to be impossible to introduce the phenomenon of growing pores in a densification model; hence the only way to discover this effect for a certain given microstructure would be by numerical simulation of the representative unit cell.

More details about numerical results of simulating representative unit cells numerically will be provided in an accompaning paper, cf. Van de Vorst [29].

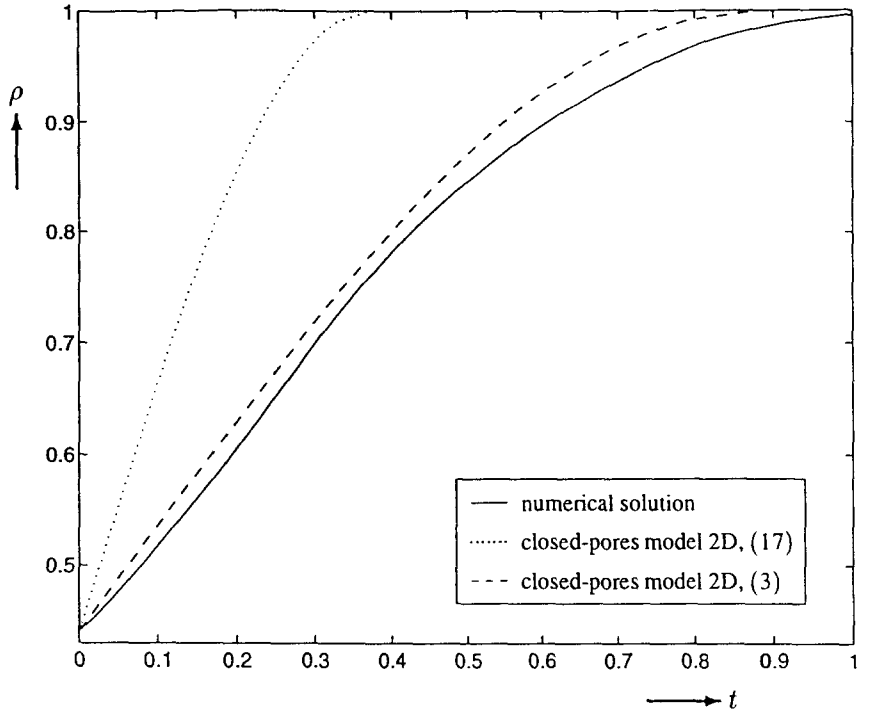

Fig. 10. The numerical densification rate of the aerogel texture of figure 9 is compared with the two-dimensional closed pores model prediction. Again, a good matching is obtained when in this model only the significantly largest pores of the unit cell are taken (3) compared with the case when all the pores are counted (17).

Acknowledgements

The author would like to express his appreciation to Dr. G.W. Scherer of DuPont de Nemours & Co. and Prof. C. Pozrikidis of the University of California at San Diego for giving useful comments on preliminary versions of this work.

References

1. H.K. Kuiken, Viscous sintering: the surface-tension-driven flow of a liquid form under the influence of curvature gradients at its surface. *J. Fluid Mech.* 214 (1990) 503–515.
2. G.A.L. van de Vorst, *Modelling and Numerical Simulation of Viscous Sintering*. PhD thesis, Eindhoven University of Technology. (1994) 181 pp.
3. C.J. Brinker and G.W. Scherer, *Sol-Gel Science: The Physics and Chemistry of Sol-Gel Processing*. London: Academic Press (1990).
4. J. Frenkel, Viscous flow of crystalline bodies under the action of surface tension. *J. Phys. USSR* 9 (1945) 385–391.
5. R.W. Hopper, Plane Stokes flow driven by capillarity on a free surface. *J. Fluid Mech.* 213 (1990) 349–375.
6. R.W. Hopper, Plane Stokes flow driven by capillarity on a free surface, 2: further developments. *J. Fluid Mech.* 230 (1991) 355–364.
7. R.W. Hopper, Stokes flow of a cylinder and half-space driven by capillarity. *J. Fluid Mech.* 243 (1992) 171–181.
8. J.W. Ross, W.A. Miller and G.C. Weatherly, Dynamic computer simulation of viscous flow sintering kinetics. *J. Appl. Phys.* 52 (1981) 3884–3888.
9. A. Jagota and P.R. Dawson, Micromechanical modeling of powder compacts-I. unit problems for sintering and traction-induced deformation. *Acta. Metall.* 36 (1988) 2551–2561.
10. A. Jagota and P.R. Dawson, Micromechanical modeling of powder compacts-II. truss formulation of discrete packings. *Acta. Metall.* 36 (1988) 2563–2573.

11. A. Jagota and P.R. Dawson, Simulation of the viscous sintering of two particles. *J. Am. Ceram. Soc.* 73 (1990) 173–177.
12. G.A.L. van de Vorst, R.M.M. Mattheij and H.K. Kuiken, Boundary element solution for two-dimensional viscous sintering. *J. Comput. Phys.* 100 (1992) 50–63.
13. G.A.L. van de Vorst and R.M.M. Mattheij, Numerical analysis of a 2-D viscous sintering problem with non smooth boundaries. *Computing* 49 (1992) 239–263.
14. G.A.L. van de Vorst, Integral method for a two-dimensional Stokes flow with shrinking holes applied to viscous sintering. *J. Fluid Mech.* 257 (1993) 667–689.
15. G.A.L. van de Vorst and R.M.M. Mattheij, A BEM–BDF scheme for curvature driven moving Stokes flows. *J. Comput. Phys.* (1995). (To appear).
16. H.A. Lorentz, Eene algemeene stelling omtrent de beweging eener vloeistof met wrijving en eenige daaruit afgeleide gevolgen. *Versl. Akad. Wetensch. Amsterdam* 5 (1896) 168–175.
17. G. de With, Meso-modelling: a proposed attempt to obtain an industrially applicable sintering theory. In: *Proc. Conf. on Modelling of Sintering Processes.* (1990). Lecture at the 71 WE Heraeus Seminar.
18. J.K. Mackenzie and R. Shuttleworth, A phenomenological theory of sintering. *Proc. Phys. Soc. Lond.* 62 (1949) 833–852.
19. G.W. Scherer, Sintering of low-density glasses: I, Theory. *J. Am. Ceram. Soc.* 60 (1977) 236–239.
20. H. Hasimoto, On the periodic fundamental solutions of the Stokes equations and their application to viscous flow past a cubic array of spheres. *J. Fluid Mech.* 5 (1959) 317–328.
21. J.F. Brady, R.J. Phillips, J.C. Lester and G. Bossis, Dynamic simulation of hydrodynamically interacting suspensions. *J. Fluid Mech.* 195 (1988) 257–280.
22. C. Pozrikidis, On the transient motion of ordered suspensions of liquid drops. *J. Fluid Mech.* 246 (1993) 301–320.
23. B.R.A. Nijboer and F.W. de Wette, On the calculation of lattice sums. *Physica* 23 (1957) 309–321.
24. M. Abramowitz and I.A. Stegun. *Handbook of Mathematical Functions.* New York: Dover Publications. (1964) 1046 pp.
25. D.C. Champeney, *Fourier Transforms and their Physical Applications.* London: Academic Press. (1973) 256 pp.
26. C.W.J. Beenaker, Ewald sum of the Rotne–Prager tensor. *J. Chem. Phys.* 85 (1986) 1581–1582.
27. G.K. Batchelor. *An Introduction to Fluid Dynamics.* Cambridge: Cambridge University Press. (1967) 605 pp.
28. A. Craievich, M.A. Aegerter, D.I. dos Santos, T. Woignier and J. Zarzycki, A SAXS Study of Silica Aerogels. *J. Non-Cryst. Solids* 86 (1986) 394–406.
29. G.A.L. van de Vorst, Numerical Simulation of Viscous Sintering by a Periodic Lattice of a Representative Unit Cell (1995). (In preparation).